

C IV Absorbers in $z > 4$ Quasars: Tracing Early Galactic Halos Evolution

Céline Péroux^{1*}, Patrick Petitjean^{2,3}, Bastien Aracil², Mike Irwin⁴ & Richard G. McMahon⁴

¹Osservatorio Astronomico di Trieste, Via Tiepolo, 11, 34 131 Trieste, Italy

²Institut d'Astrophysique de Paris, 98 bis Bld Arago, 75 014 Paris, France

³LERMA, Observatoire de Paris, 61 avenue de l'Observatoire, 75 014 Paris, France

⁴Institute of Astronomy, Madingley Road, Cambridge CB3 0HA, UK

11th December 2018

Abstract We use 29 $z > 4$ quasar spectra to build a homogeneous sample of high-redshift C IV absorbers. We use these data to calculate the number density, $n(z)$, of $W_{\text{rest}}(\text{C IV}) > 0.30\text{\AA}$ C IV doublets. We find that $n(z)$ increases with time from $z \sim 4.5$. In addition, $W_{\text{rest}}(\text{C IV}) > 0.15\text{\AA}$ C IV systems are more numerous than the former at all redshifts. On the contrary, $n(z)$ of $W_{\text{rest}}(\text{Mg II}) > 0.30\text{\AA}$ Mg II doublets decreases with time, in agreement with results from studies of LLS number densities. Below $z < 3$, none of all the classes of absorbers show signs of evolution. We interpret this as the formation of galactic envelopes from smaller halos. Furthermore, the doublet ratio $\text{DR} = W(\text{C IV } 1548)/W(\text{C IV } 1550)$ is found to decrease with time, a signature of the increase of the mean C IV column density. Finally, the $W(\text{Si IV } 1393)/W(\text{C IV } 1548)$ ratios in strong absorbers ($W_{\text{rest}}(\text{C IV } 1548) \geq 0.50\text{\AA}$) is found to be approximately constant from $z = 3.5$ to $z = 2.5$ and then to decrease with time. This result suggests that the highest column density absorbers are not sensitive to changes in the ionization continuum.

Key words. Cosmology: observations – Galaxies: evolution – Quasars: absorption lines – Galaxies: halos – Galaxies: high-redshift

1. Introduction

Various lines of evidence point towards a direct connection between metal-line absorption systems observed in the spectra of high redshift background quasars and normal galaxies. Mg II systems are known to be associated with the gaseous envelopes of bright galaxies which have been detected in emission at $z \sim 0.6$ (Bergeron & Boissé 1991). The typical impact parameter from the galaxy varies with the equivalent width threshold of the surveys for absorbers: $40\text{ h}^{-1}\text{ kpc}$ at $W_{\text{rest}} = 0.30\text{\AA}$ and $60\text{ h}^{-1}\text{ kpc}$ at $W_{\text{rest}} = 0.02\text{\AA}$ (Churchill et al. 1999). In addition the absorbers optically thick to hydrogen ionizing radiation, i.e. neutral hydrogen absorbers with $N(\text{HI}) > 10^{17.2}\text{ cm}^{-2}$, the Lyman limit systems (hereafter LLS) have sizes comparable to the $W_{\text{rest}} = 0.30\text{\AA}$ Mg II selected systems. Therefore both Mg II and LLS are believed to arise from the same type of object.

At $z < 1$, C IV absorbers arise from the extended ($100\text{ h}^{-1}\text{ kpc}$) halos of galaxies of a wide range of luminosity and morphological type (Chen, Lanzetta & Webb 2001). More specifically, Adelberger et al. (2003) have shown that at $z \sim 3$, all C IV absorbers are situated within $200\text{ h}^{-1}\text{ kpc}$ of a Lyman-break galaxy and argue that this distance is characteristic of

a galactic-scale outflow driven by star formation activity in this type of galaxy. Moreover, simulations have shown that the observed C IV kinematic structure and column densities can be well reproduced by merging of proto-galactic clumps (Haehnelt, Steinmetz & Rauch 1996). Compact halos of hot gas with temperature close to $\sim 10^5\text{ K}$ satisfactorily explain the observed multi-component nature of the C IV absorbers. These absorption systems thus provide a powerful observational tool to understand the processes of galaxy formation and evolution that deposit chemically enriched material far from the central galaxy.

The methods used to study the properties of C IV systems can be split into two different approaches. First, observing C IV in high signal-to-noise ratio, high-resolution spectra, allows us to determine their column density down to $\log N(\text{C IV}) \sim 11.8\text{ cm}^{-2}$. This enables detailed kinematic and temperature studies (Rauch et al. 1996) which show that C IV components may be the building blocks of future normal galaxies. Such data are also used to determine the low end of the C IV column density distribution (Ellison et al. 2000) and mass density (Songaila 2001; Pettini et al. 2003; Boksenberg, Sargent & Rauch 2003) and to study the velocity structure within the halos (e.g. Petitjean & Bergeron 1994 and Crotts, Burles & Tytler

* Marie Curie Fellow. E-mail: peroux@ts.astro.it

1997). Nevertheless, such analysis are currently limited to a few lines of sight.

The second approach consists in studying a statistically significant number of absorbers by constructing a large homogeneous sample. Steidel (1990) uses quasar spectra at $3.04 < z_{\text{em}} < 4.11$ in addition to data at $1.08 < z_{\text{em}} < 3.56$ from Sargent, Boksenberg & Steidel (1988) to build such a homogeneous sample. They find that the number density of CIV systems, $n(z)$, increases with increasing redshift in the range $z_{\text{abs}} = 1,3 - 3.7$ and deduce from this that the properties of the absorbers are evolving with time. Using a two-point correlation function to study the clustering of the CIV doublets, they find marginal evidence that the width of the correlation peak on small velocity scales is smaller at high redshift than in the local Universe. Quashnock, Vanden Berk & York (1996) show that clustering is also present at higher redshift, although its scale does not appear to have changed significantly since then. More recently, Misawa et al. (2002) have used higher-resolution spectra (2 Å FWHM) from the Keck telescope to conduct a systematic search for CIV doublets. They measure $n(z)$ up to $z \sim 4$ and find that their results agree with Steidel (1990) at a rest equivalent width limit of $W_{\text{rest}} = 0.30$ Å, but not at $W_{\text{rest}} = 0.15$ Å. We propose here that this discrepancy is actually due to incompleteness in the Steidel sample at $W_{\text{rest}} > 0.15$ Å linked with the lower resolution of the survey and pay particular attention to this point in our analysis.

Although both these approaches are complementary, the paucity of strong CIV systems means that the second technique is more appropriate to study the characteristics and evolution of the galactic halos. In the present study, we use 29 $z > 4$ quasar spectra to build a new and homogeneous sample of high-redshift CIV absorbers. In section 2, we summarise the set-up for the observations and detail the data reduction process in section 3. The method for the identification of the absorbers is presented in section 4 together with a list of CIV systems. The statistical properties of this sample are derived in section 5 and discussed in section 6. This paper assumes $\Omega_{\Lambda} = 0.7$ and $\Omega_0 = 0.3$ throughout.

2. Observations

All the quasars observed in the present study were selected from the lower-resolution survey of Péroux et al. (2001). The new observations were carried out during two observing runs at the 4.2 m William Herschel telescope (WHT) of the Isaac Newton Group of telescopes in the Canary Islands and two observing runs at the 3.58 m New Technology Telescope (NTT) of the European Southern Observatory in La Silla, Chile. High signal-to-noise optical spectrophotometry was obtained covering approximately 7000 Å to 8000 Å, the exact range depending on which instrument was used for the observations. A journal of the observations is presented in Table 1.

Eleven quasars were observed at the WHT during 2001 November 7 – 8 and 2002 June 1 – 2. The first run suffered bad weather conditions, thus limiting the number of objects observed and the quality of the resulting spectra. The integration times ranged from 1200 – 7200 seconds. We used only the red arm of the ISIS spectrograph. A new CCD was installed before

the second run took place and therefore the characteristics of the set-ups slightly changed between the two observational sessions. For the November run a thinned coated Tektronix CCD was used, while a thinned coated EEV CCD was used for the June run. Grating R600R was used leading to a dispersion of 0.79 Å pixel⁻¹ for the November run and 0.44 Å pixel⁻¹ for the June run. In all cases, a GG495 blocking filter was used to minimize the second order contamination. All the observations were taken with a slit width of 1.0 – 1.5 arcsec. Blind-offsetting from bright ~ 15 – 17^{th} magnitude stellar fiducials was used to position the quasars in the slit, partly to save acquisition time and partly because the majority of the quasars were not visible using the blue sensitive TV acquisition system. Readout time was reduced by windowing the CCDs in the spatial direction.

Eighteen quasars (including the possibly BAL quasar PSS J1723+2243) were observed at the NTT during 2001 December 16 – 18 and 2002 August 11 – 13 using the ESO Multi-Mode Instrument (EMMI). The exposure times ranged from 3600 to 10800 seconds. Again, a new CCD was installed before the second run took place and therefore the characteristics of the set-ups slightly changed between the two observational sessions. For the December run a thin, back-illuminated Tektronix CCD was used, while a MIT/LL CCD was used for the August run. Grating #7 used on both occasions and gave dispersions of 0.66 Å pixel⁻¹ for the December run and 0.82 Å pixel⁻¹ for the August run. In both cases a OG530#645 blocking filter was used to minimize the second order contamination. All the observations were taken with a slit width of ~ 1.0 arcsec. Readout time was again reduced by windowing the CCDs in the spatial direction.

3. Data Reduction

The data reduction was undertaken using the IRAF¹ software package. Because the bias frames for each nights were so similar, a master ‘zero’ frame for each run was created using the IMCOMBINE routine. The data were overscan-corrected, zero-corrected, and trimmed using CCDPROC. Similarly, a single flat-field frame was produced by taking the median of the (suitably scaled) flats. The overall background variation across this frame was removed to produce an image to correct for the pixel-to-pixel sensitivity variation of the data. The task APALL was used to extract 1-D multi-spectra from the 2-D frames. The routine estimates the sky level by model fitting over specified regions on either side of the spectrum. In the cases where the objects were faint on the 2-D frames, different exposures were IMCOMBINED before extraction with APALL.

The WHT data were wavelength calibrated using CuAr and CuNe arcs and the NTT data using HeAr and Ar lamps. Night sky lines were used to monitor the wavelength calibration for all spectra. In all but one run, observations of B-stars free of strong features in the red were taken in order to remove the effects of atmospheric absorption (e.g. O₂ A band at 7600 Å)

¹ IRAF is distributed by the National Optical Astronomy Observatories, which are operated by the Association of Universities for Research in Astronomy, Inc., under cooperative agreement with the National Science Foundation.

Quasar Name	z_{em}	APM R Mag	Telescope	Date	Exp. Time (sec)	Spectral Coverage
BR J0006–6208	4.455	18.3	NTT	2002 Aug	9000	7008–8512
BR J0030–5129	4.174	18.6	NTT	2002 Aug	7500	6508–8016
PSS J0034+1639	4.293	18.0	NTT	2002 Aug	6000	6611–8117
PSS J0133+0400	4.154	18.3	NTT	2002 Aug	9000	6365–7860
PSS J0248+1802	4.422	17.7	WHT	2001 Nov	3300	6631–7442
BR J0311–1722	4.039	17.7	NTT	2001 Dec	3600	6500–7820
BR J0324–2918	4.622	18.7	NTT	2001 Dec	10800	7150–8470
BR J0334–1612	4.363	17.9	WHT	2001 Nov	1800	6631–7442
BR J0355–3811	4.545	17.9	NTT	2001 Dec	3600	7150–8470
BR J0419–5716	4.461	17.8	NTT	2001 Dec	5400	7150–8470
BR J0426–2202	4.320	17.9	NTT	2001 Dec	6000	6930–8250
PMN J0525–3343	4.383	18.4	NTT	2001 Dec	9000	6930–8250
BR J0529–3552	4.172	18.3	NTT	2001 Dec	9000	6500–7820
BR J0714–6455	4.462	18.3	NTT	2001 Dec	9000	7150–8470
PSS J0747+4434	4.430	18.4	WHT	2001 Nov	1200	6631–7442
PSS J1159+1337	4.073	17.1	WHT	2002 Jun	4500	6000–7400
PSS J1253–0228	4.007	18.8	WHT	2002 Jun	6300	6000–7400
PSS J1330–2522	3.949	18.5	WHT	2002 Jun	5400	6000–7400
BR J1456+2007	4.249	18.2	WHT	2002 Jun	7200	6850–8350
BR J1618+4125	4.213	18.5	WHT	2002 Jun	7200	6850–8350
PSS J1633+1411	4.351	18.7	NTT	2002 Aug	10800	7008–8512
PSS J1646+5514	4.037	17.1	WHT	2002 Jun	4500	6850–8350
PSS J1723+2243*	4.520	18.2	NTT	2002 Aug	3600	7008–8512
PSS J1802+5616	4.158	18.3	WHT	2002 Jun	6300	6850–8350
PSS J2154+0335	4.363	19.0	NTT	2002 Aug	10800	6615–8117
PSS J2155+1358	4.256	18.0	WHT	2002 Jun	6300	6850–8350
BR J2216–6714	4.469	18.6	NTT	2002 Aug	10200	7008–8512
PSS J2344+0342	4.239	18.2	NTT	2002 Aug	9600	6510–8010
BR J2349–3712	4.208	18.7	NTT	2002 Aug	10200	6510–8010

*Object possibly affected by BAL features.

Table 1. Journal of Observations.

in the quasar spectra. No such observations were made in the December run at NTT, and therefore in this case appropriately scaled B-star spectra were used for atmospheric correction. The atmospheric absorption features seen in the B-star spectrum were isolated by interpolating between values on either side of the feature. The original B-star spectrum was then divided by this atmospheric-free spectrum to create an atmospheric correction spectrum. Finally the object spectra were divided by the scaled correction spectrum.

The resolution of the resulting spectra ranges from 1.60 to 2.30Å. An estimate of the continuum signal-to-noise ratio is given in Table 3 for each object. The spectra are shown in Figure 1 with arbitrary flux scales. The quasar redshifts and magnitudes listed in Table 1 are from the original survey of Péroux et al. (2001). All the spectra were then continuum normalised within the MIDAS data reduction software package (Fontana & Ballester 1995) in order to detect the signature of intervening absorption lines. For this purpose a spline function was fitted to the quasar continuum to smoothly connect the regions free from absorption features, as is standard practice.

4. Metal Identification

4.1. Methodology

To select metal lines we use a detection algorithm based on the method presented in Péroux et al. (2001), supplemented by a visual search. Following past work, the spectra are analysed from 5000 km s⁻¹ blueward of the C IV emission line (to avoid lines possibly associated with the quasar) towards shorter wavelengths. The analysis is stopped when the signal-to-noise ratio becomes too low to detect a C IV line at the 5 σ level (corresponding to z_{min} in Table 3). We then calculate the equivalent widths of all the candidate lines. Figure 2 shows an example (for PSS J1159+1337) of the output of the algorithm we use to detect metal lines - a box-like running average of the equivalent width as a function of wavelength. In this figure, our detection threshold is represented by the straight dashed line: any feature peaking above this limit is a candidate absorber. This output is then visually inspected to detect any lines which might have been missed by the automatic procedure. The lines are then identified by analysing each spectrum in velocity space and the redshift of the system is measured that best fits each line of a doublet and other associated lines. All detected absorptions with confirmed identifications are listed in Table A.1 of the appendix for each quasar spectrum.

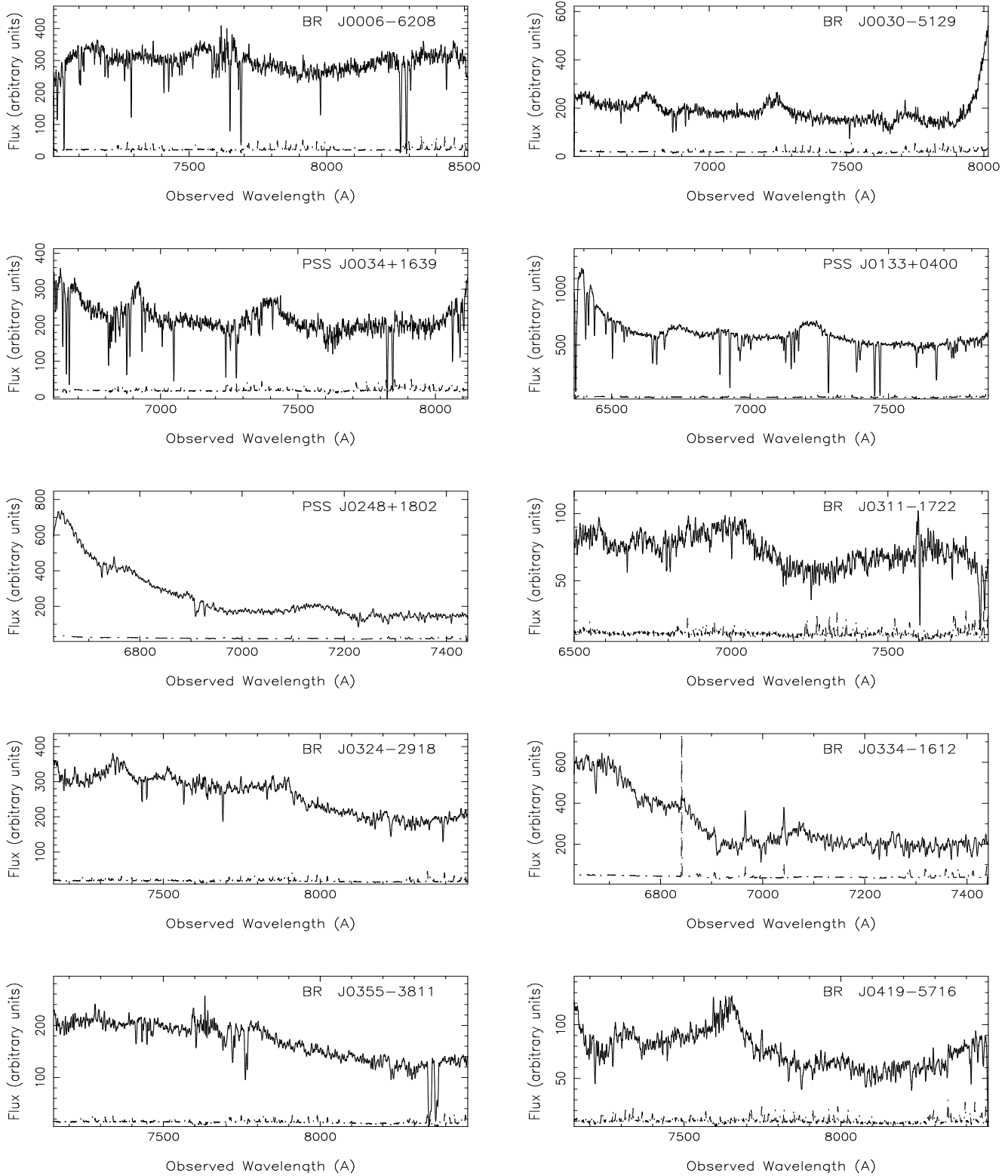


Figure 1. Spectra of the 29 $z > 4$ quasars observed as part of the survey.

4.2. Notes on Individual Spectra

1. BR J0006-6208 ($z_{\text{em}} = 4.455$)

$z_{\text{abs}} = 1.687$ – Weak absorption but the wavelength alignment and EW ratio are in excellent agreement with expectations from Mg II absorbers.

$z_{\text{abs}} = 1.956$ – Symmetric profiles associated with a saturated Mg II doublet. Mg I 2852 and many associate Fe II lines (2374, 2382, 2586, 2600) are observed. Possible Fe I 2719 and Si I 2515 are also found at the same redshift.

$z_{\text{abs}} = 3.588$ – Unambiguous two-component CIV doublet with possible associate C I 1560.

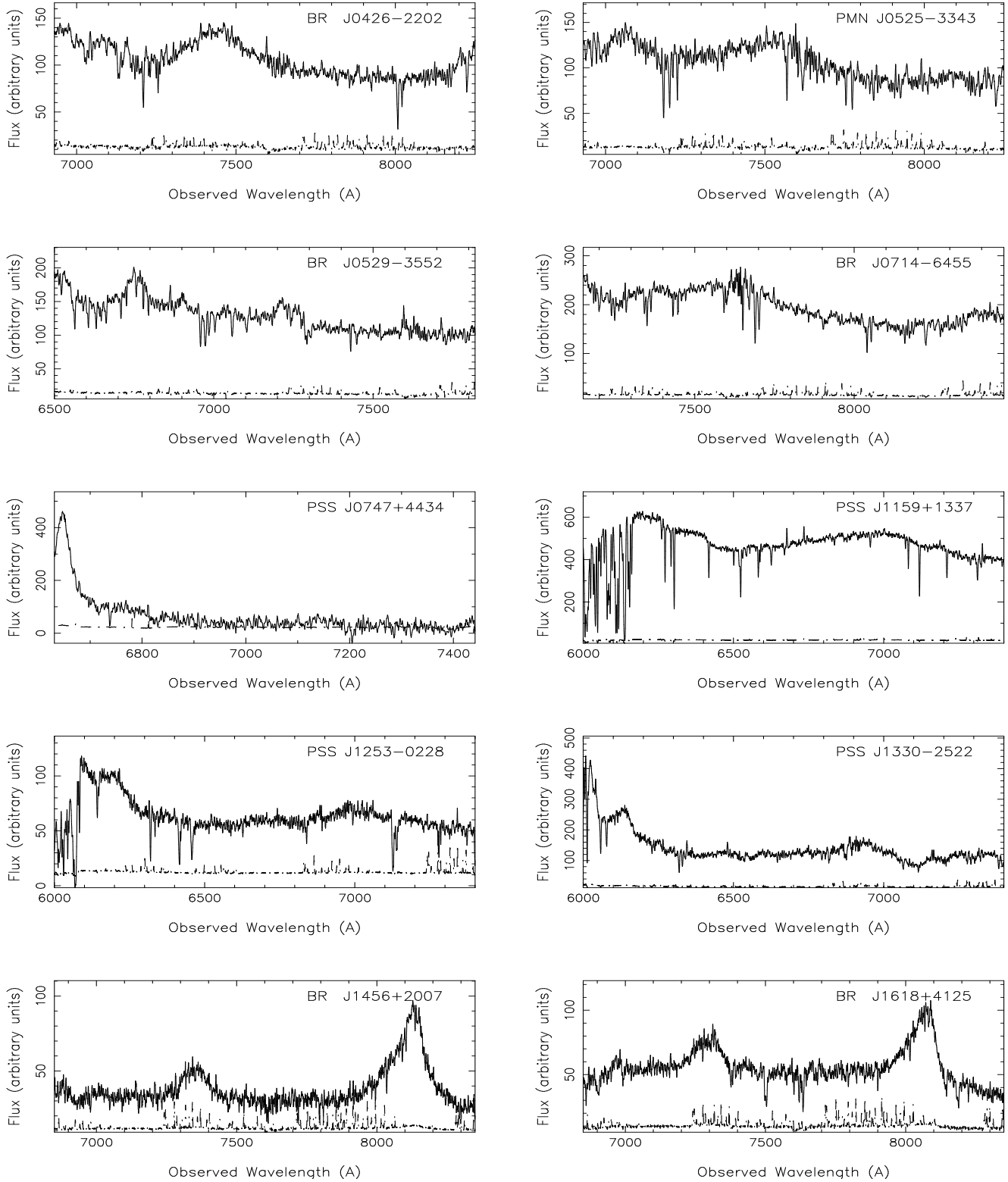


Figure 1. *Continued.*

2. BR J0030-5129 ($z_{\text{em}} = 4.174$)
 $z_{\text{abs}} = 3.465$ – Narrow, well-defined CIV doublet.
3. PSS J0034+1639 ($z_{\text{em}} = 4.293$)
 $z_{\text{abs}} = 1.588$ – The two members of this Mg II doublet are not exactly aligned, but EW ratio means that this is a definite identification.

$z_{\text{abs}} = 1.798$ – The 2796 line of this Mg II doublet is saturated. Associated strong Fe II 2382, 2586 and 2600 lines are observed.

$z_{\text{abs}} = 1.883$ – The 2803 line of this Mg II doublet is slightly contaminated on its red side by CIV 1548 at $z_{\text{abs}} = 4.225$.

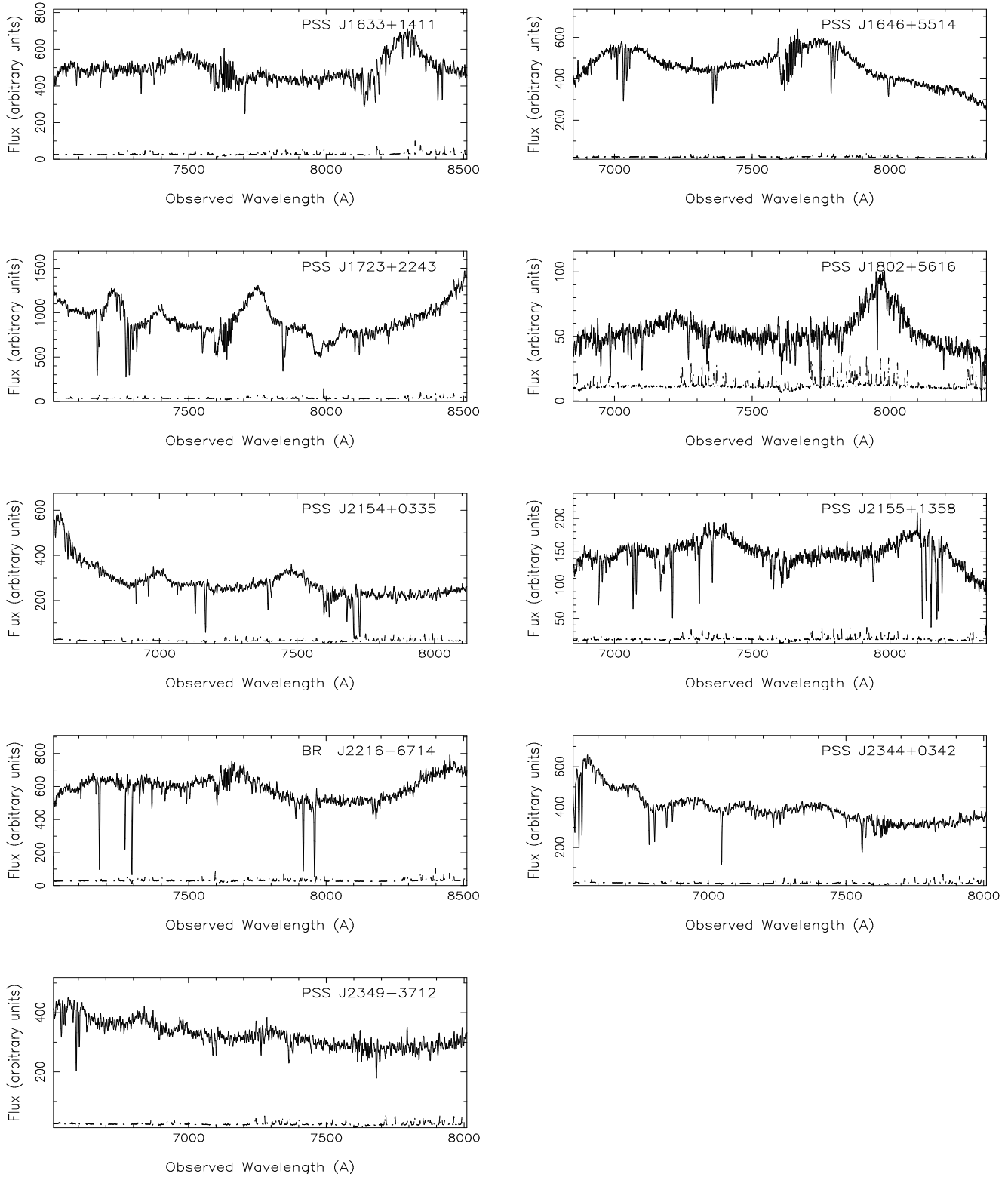


Figure 1. *Continued.*

$z_{\text{abs}} = 3.442$ – Although the EW ratio is not precisely the one expected from CIV doublets, the wavelength alignment and similarity in profiles mean that this is most probably a CIV absorption. CI 1560 coincides exactly with the CIV 1548 at $z_{\text{abs}} = 3.478$.

$z_{\text{abs}} = 3.478$ – Clean and unambiguous CIV doublet with associated Si II 1526.

$z_{\text{abs}} = 4.225$ – At red end of the spectrum, another CIV doublet is clearly detected. CI 1328 coincides exactly with the CIV 1550 at $z_{\text{abs}} = 3.478$ and Si II 1304 is detected.

4. PSS J0133+0400 ($z_{\text{em}} = 4.154$)

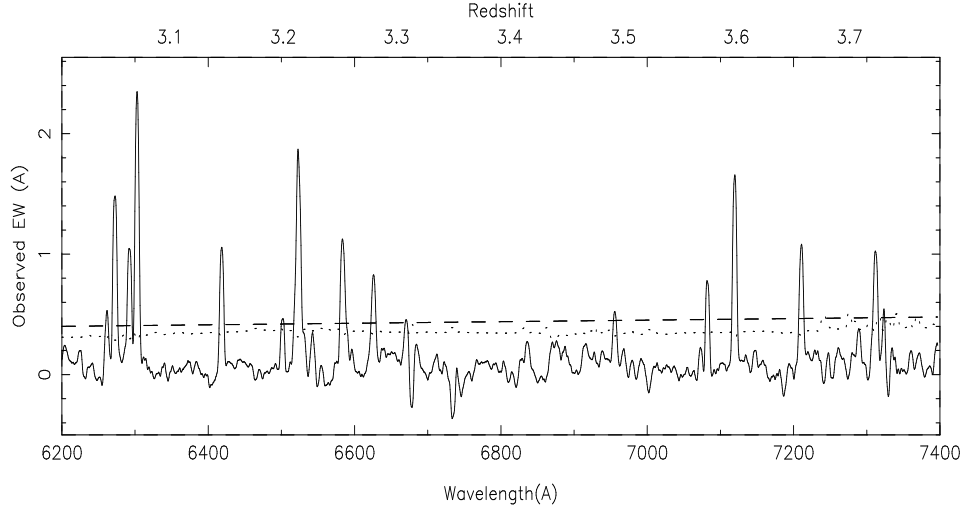


Figure 2. Example of the output of the automated metal line search (for quasar PSS J1159+1337). The solid line corresponds to the equivalent width spectrum and the dotted line to the error array. The straight dashed line represents the threshold above which the candidate absorbers are selected. An example is the $z_{\text{abs}} = 3.724$ C IV doublet clearly visible at $\lambda_{\text{obs}} \sim 7300\text{\AA}$ and the corresponding Si IV doublet situated at $\lambda_{\text{obs}} \sim 6600\text{\AA}$.

This spectrum is particularly rich in Si IV doublets.

$z_{\text{abs}} = 1.664$ – Saturated Mg II doublet with associated Mg I 2852 absorption line. Fe II 2586 and 2600 are also observed at this redshift.

$z_{\text{abs}} = 3.138$ – Although contamination between the two lines of this C IV doublet means that the EW ratio is slightly off the expected value, this is most probably a C IV system.

$z_{\text{abs}} = 3.229$ – Small, well-defined C IV doublet.

$z_{\text{abs}} = 3.620$ – This Si IV doublet might have associated C IV absorption, but given the sky contamination at the relevant wavelengths (around 7150 Å), this cannot be confirmed.

$z_{\text{abs}} = 3.771$ – This C IV doublet is characterised by an asymmetric profile which is also seen in Si IV. A strong C II 1334 is observed at the blue end of the spectrum and additional Si II 1526 and Fe II 1608 are detected at the same redshift. Péroux et al. (2001) also report a DLA at this redshift.

$z_{\text{abs}} = 3.992$ – C IV system with associated a Si IV doublet.

$z_{\text{abs}} = 3.996$ – Situated only 300 km s^{-1} away from the previous system, this C IV doublet has associated with O I 1302 and Si II 1304 absorptions.

$z_{\text{abs}} = 4.110$ – Narrow Si IV doublet with a possible C I 1280 line associated and a definite Si II 1304 feature (C I 1280 is blended with C IV 1548 at $z_{\text{abs}} = 3.229$).

$z_{\text{abs}} = 4.115$ – Situated only 300 km s^{-1} away from the previous system, this is another narrow Si IV doublet with associated Si II 1526.

5. PSS J0248+1802 ($z_{\text{em}} = 4.422$)

$z_{\text{abs}} = 1.470$ – Although Mg II 2796 is contaminated on its red wing, this is most probably a Mg II doublet.

$z_{\text{abs}} = 3.969$ – Si IV doublet with Si IV 1393 blended with Mg II 2803 at $z_{\text{abs}} = 1.470$.

$z_{\text{abs}} = 4.185$ – Another medium-strength Si IV doublet.

6. BR J0311–1722 ($z_{\text{em}} = 4.039$)

$z_{\text{abs}} = 4.034$ – This definite C IV doublet has an asymmetric profile. O I 1302 is possibly detected at the same redshift.

7. BR J0324–2918 ($z_{\text{em}} = 4.622$)

$z_{\text{abs}} = 1.923$ – Weak Mg II doublet.

$z_{\text{abs}} = 2.227$ – Many Fe II lines (2344, 2382, 2586 and 2600) are detected at this redshift, but our spectrum does not cover the appropriate wavelength range for the detection of the Mg II doublet.

$z_{\text{abs}} = 3.746$ – Weak C IV doublet.

8. BR J0334–1612 ($z_{\text{em}} = 4.363$)

$z_{\text{abs}} = 3.668$ – Narrow C IV doublet.

$z_{\text{abs}} = 3.759$ – Another narrow C IV doublet.

$z_{\text{abs}} = 3.788$ – A Si IV doublet is detected at this wavelength.

$z_{\text{abs}} = 4.186$ – Another Si IV doublet is detected, with the Si IV 1393 line blended with C IV 1548 at $z_{\text{abs}} = 3.668$.

9. BR J0355–3811 ($z_{\text{em}} = 4.545$)

$z_{\text{abs}} = 1.986$ – This saturated Mg II doublet shows clear evidences of a two-component profile. Associated Fe II 2586 and 2600 lines are observed.

$z_{\text{abs}} = 3.855$ – Unusually broad and weak C IV doublet.

$z_{\text{abs}} = 4.313$ – Weak C IV doublet.

$z_{\text{abs}} = 4.318$ – Situated 300 km s^{-1} away from the previous system, another weak C IV system.

10. BR J0419–5716 ($z_{\text{em}} = 4.461$)

$z_{\text{abs}} = 2.028$ – Many Fe II lines (2382, 2586 and 2600) are detected at this redshift, but our spectrum does not cover the appropriate wavelength range for the detection of the Mg II doublet.

$z_{\text{abs}} = 4.218$ – The C IV 1550 line of this doublet is probably contaminated by another absorption, which explains the differences in the profile shape of this C IV doublet.

- $z_{\text{abs}} = 4.311$ – Unambiguous CIV doublet.
 $z_{\text{abs}} = 4.434$ – Weak CIV doublet where the CIV 1548 line is blended with a stronger unidentified absorption.
11. BR J0426–2202 ($z_{\text{em}} = 4.320$)
 $z_{\text{abs}} = 3.606$ – This CIV doublet shows a characteristic two-component profile.
 $z_{\text{abs}} = 3.682$ – Weak CIV doublet.
 $z_{\text{abs}} = 4.172$ – Nicely defined CIV doublet with associated Si IV absorption.
12. PMN J0525–3343 ($z_{\text{em}} = 4.383$)
 $z_{\text{abs}} = 1.568$ – Well defined Mg II doublet.
 $z_{\text{abs}} = 3.581$ – Weak CIV doublet with associated Fe II 1608 absorption.
 $z_{\text{abs}} = 4.063$ – Weak CIV doublet with associated Si IV doublet (the Si IV 1402 is blended with CIV 1548 at $z_{\text{abs}} = 3.581$), Si II 1526 and Fe II 1608.
 $z_{\text{abs}} = 4.313$ – Slightly broad CIV doublet.
 $z_{\text{abs}} = 4.430$ – Si IV doublet.
13. BR J0529–3552 ($z_{\text{em}} = 4.172$)
 $z_{\text{abs}} = 1.398$ – Fairly weak Mg II doublet.
 $z_{\text{abs}} = 1.423$ – The profile of this Mg II doublet is characterised by a square shape.
 $z_{\text{abs}} = 1.656$ – Another Mg II doublet is observed at this redshift.
 $z_{\text{abs}} = 3.503$ – Well defined CIV doublet with associated Fe II 1608 and Al II 1670 absorption lines.
 $z_{\text{abs}} = 4.062$ – This Si IV doublet is accompanied with Si II 1304 & 1526 and C II 1304.
14. BR J0714–6455 ($z_{\text{em}} = 4.462$)
 $z_{\text{abs}} = 3.747$ – This CIV doublet is associated with a Si II 1526 line.
 $z_{\text{abs}} = 3.966$ – Another well defined CIV doublet is detected at this redshift.
 $z_{\text{abs}} = 4.193$ – Both CIV and Si IV doublets are observed, but Si IV 1402 is blended with Si II 1526 at $z_{\text{abs}} = 3.747$.
15. PSS J0747+4434 ($z_{\text{em}} = 4.430$)
This spectrum is of very low quality and no lines could be identified.
16. PSS J1159+1337 ($z_{\text{em}} = 4.073$)
 $z_{\text{abs}} = 1.739$ – Many Fe II lines (2344, 2374, 2382, 2586 and 2600) are detected at this redshift, but our spectrum does not cover the appropriate wavelength range for the detection of the Mg II doublet.
 $z_{\text{abs}} = 3.724$ – CIV and Si IV doublets are detected at this redshift (the Si IV line is blended with Si IV 1393 at 3.756). Péroux et al. (2001) also report a DLA at this redshift.
 $z_{\text{abs}} = 3.756$ – Another Si IV doublet is observed.
17. PSS J1253–0228 ($z_{\text{em}} = 4.007$)
 $z_{\text{abs}} = 1.261$ – A strong Mg II doublet is detected at this redshift.
 $z_{\text{abs}} = 3.606$ – This CIV doublet also shows strong Si IV doublet and C II 1334 line with the same characteristic two component profile. Péroux et al. (2001) also report a sub-DLA (see Péroux et al. 2003 for a definition of this class of systems) at this redshift.
18. PSS J1330–2522 ($z_{\text{em}} = 3.949$)
 $z_{\text{abs}} = 3.084$ – Associated with this CIV doublet is Al II 1670. Péroux et al. (2001) also report a sub-DLA (see Péroux et al. 2003) at this redshift.
 $z_{\text{abs}} = 3.390$ – Another CIV doublet is observed at this redshift.
 $z_{\text{abs}} = 3.772$ – A weak Si IV doublet is detected.
 $z_{\text{abs}} = 3.769$ – At the red end of the spectrum, another CIV doublet is detected.
19. BR J1456+2007 ($z_{\text{em}} = 4.249$)
 $z_{\text{abs}} = 1.761$ – Narrow Mg II doublet.
 $z_{\text{abs}} = 4.036$ – The CIV 1550 line of this CIV doublet is slightly contaminated.
20. BR J1618+4125 ($z_{\text{em}} = 4.213$)
 $z_{\text{abs}} = 4.223$ – This Si IV system is the only doublet which can be convincingly identified.
21. PSS J1633+1411 ($z_{\text{em}} = 4.351$)
 $z_{\text{abs}} = 3.580$ – Nice CIV doublet
 $z_{\text{abs}} = 4.150$ – A Si IV doublet is identified at this redshift.
 $z_{\text{abs}} = 4.282$ – This CIV doublet has a characteristic profile which includes a smaller component to the blue of the main feature.
22. PSS J1646+5514 ($z_{\text{em}} = 4.037$)
This spectrum is particularly rich in CIV systems which are visible as clustered pairs of doublets.
 $z_{\text{abs}} = 1.859$ – Well defined Mg II doublet where the EW ratio is in excellent agreement with expectations from physical properties.
 $z_{\text{abs}} = 3.516$ – A weak CIV doublet is detected at this redshift.
 $z_{\text{abs}} = 3.521$ – This medium strength CIV system has its CIV 1548 line blended with the CIV 1550 line at $z_{\text{abs}} = 3.544$.
 $z_{\text{abs}} = 3.544$ – In the close vicinity of the previous system is another stronger CIV doublet.
 $z_{\text{abs}} = 3.754$ – This CIV doublet has its lines separated by the CIV 1548 line at $z_{\text{abs}} = 3.759$.
 $z_{\text{abs}} = 3.759$ – This weaker CIV doublet is crossing the previous doublet but can nevertheless be fairly well isolated for EW measurements.
 $z_{\text{abs}} = 4.030$ – Similarly to the two doublets described above, this CIV system is crossed over by the $z_{\text{abs}} = 4.037$ CIV absorber, although the closer proximity between the two means that the EW are not as reliable. The Si IV doublet, Si II 1526 and Fe II 1608 are also detected at this redshift.
 $z_{\text{abs}} = 4.037$ – Weaker CIV absorber as described above.
23. PSS J1723+2243 ($z_{\text{em}} = 4.520$)
 $z_{\text{abs}} = 3.696$ – Characteristic two-component Si II 1526, Fe II 1608 and Al II 1670 are detected at this redshift. The shape of features means that the identification is unambiguous. Nevertheless the corresponding CIV doublet is not convincing due to an odd EW ratio.
 $z_{\text{abs}} = 3.704$ – Well defined and strong CIV doublet.
 $z_{\text{abs}} = 4.234$ – This CIV doublet is blended in its CIV 1550 line with the CIV 1548 at $z_{\text{abs}} = 4.244$.
 $z_{\text{abs}} = 4.244$ – The CIV system identified at this redshift is clustered with the doublet described previously. The consequences of this arrangement is that the EW measurements

- are less reliable. Si IV is nevertheless observed at this redshift.
24. PSS J1802+5616 ($z_{\text{em}} = 4.158$)
 $z_{\text{abs}} = 4.048$ – A Si IV doublet is identified at this redshift.
 $z_{\text{abs}} = 4.190$ – A weak CIV doublet is detected at this redshift. The CIV 1548 line is probably contaminated to some extent.
25. PSS J2154+0335 ($z_{\text{em}} = 4.363$)
 $z_{\text{abs}} = 1.756$ – This saturated Mg II absorber is associated with a Mg I 2852 absorption. Fe II 2586 and 2600 are also detected at this redshift.
 $z_{\text{abs}} = 3.776$ – The good alignment and EW ratio means that this a definite CIV doublet. Nevertheless, the CIV 1550 line is clearly contaminated in its blue wing by some unidentified absorption which means that the EW measurement of this line is not reliable. Péroux et al. (2001) also report a sub-DLA (see Péroux et al. 2003) at this redshift.
 $z_{\text{abs}} = 3.961$ – Very well defined CIV doublet is observed at this redshift. The associated Si IV doublet is also detected.
26. PSS J2155+1358 ($z_{\text{em}} = 4.256$)
 $z_{\text{abs}} = 1.914$ – The characteristic two-component saturated profile is unambiguously associated with a Mg II doublet. Fe II (2382, 2586 and 2600) lines are also detected at this redshift.
 $z_{\text{abs}} = 3.567$ – Although the EW ratio of this doublet is not in excellent agreement with expectations from CIV physical properties, we identify this system as a CIV absorber.
 $z_{\text{abs}} = 4.243$ – This CIV doublet is saturated which means that the EW ratio is not reliable. The identification is nevertheless reliable. A strong Si IV doublet is also detected at this redshift.
27. BR J2216–6714 ($z_{\text{em}} = 4.469$)
 $z_{\text{abs}} = 2.060$ – Many Fe II lines (2344, 2374, 2382, 2586 and 2600) are detected at this redshift, but our spectrum does not cover the appropriate wavelength range for the detection of the Mg II doublet.
 $z_{\text{abs}} = 3.728$ – Although the profiles are quite different for the two lines of this CIV doublet, the identification is secure due to a good alignment in velocity space and an EW ratio that conforms to expectations from the physical properties of these systems.
 $z_{\text{abs}} = 3.837$ – Another CIV doublet is observed at this wavelength.
 $z_{\text{abs}} = 4.095$ – A weak CIV system is present at this redshift.
28. PSS J2344+0342 ($z_{\text{em}} = 4.239$)
 $z_{\text{abs}} = 3.219$ – This CIV doublet is probably saturated which would explain the unexpected EW ratio. Fe II 1608 and Al II 1670 are also detected at this redshift. Péroux et al. (2001) also report a DLA at this redshift.
 $z_{\text{abs}} = 4.053$ – There is a weak CIV doublet at this redshift and associated Si II 13094 and 1526 absorption lines.
 $z_{\text{abs}} = 3.882$ – Both CIV and Si IV are clearly observed at this redshift.
29. BR J2349–3712 ($z_{\text{em}} = 4.208$)

$z_{\text{abs}} = 1.758$ – Although the Mg II 2803 line of this doublet is slightly contaminated, this system is most probably a weak Mg II absorber.

$z_{\text{abs}} = 3.258$ – A CIV doublet is clearly identified at this redshift.

$z_{\text{abs}} = 3.284$ – A weak CIV system is detected at this redshift. Fe II 1608, Al II 1670 and Si II 1526 are also observed at the same redshift.

$z_{\text{abs}} = 3.690$ – Yet another CIV doublet is detected at this redshift. The Si IV doublet and Al II 1670 are also detected at this redshift. The Si IV 1393 line is blended with Si II 1526 at $z_{\text{abs}} = 3.284$. Péroux et al. (2001) also report a sub-DLA (see Péroux et al. 2003) at this redshift.

$z_{\text{abs}} = 3.756$ – A weak CIV absorber is found at this redshift, although the profiles of both lines are not totally identical.

$z_{\text{abs}} = 3.960$ – A nice CIV system is detected. It is characterised by a two-component profile.

Absorber	all	$W_{\text{rest}} > 0.15$	$W_{\text{rest}} > 0.30$	$W_{\text{rest}} > 0.70$
CIV	64	41	19	...
Mg II	19	14	11	7
Si IV	28	14	3	...

Table 2. Number of absorber for a given W_{rest} limit.

The whole sample is composed of 64 CIV 19 Mg II and 28 Si IV doublets. For comparison Steidel (1990) use 11 spectra at $3.04 < z_{\text{em}} < 4.11$ in addition to the 55 spectra at $1.08 < z_{\text{em}} < 3.56$ from Sargent, Boksenberg & Steidel (1988) and finds a total of 275 CIV. Steidel & Sargent (1992) find 111 Mg II absorbers in 103 quasar spectra. Songaila (2001) has looked for CIV and Si IV doublets in the spectra of 32 quasars with $2.31 < z_{\text{em}} < 5.86$ down to $\log(N_{\text{CIV}}) > 12.0$. She finds a total of 139 CIV lines and 49 Si IV lines at $z_{\text{abs}} > 3.5$, with 122 and 39, respectively for $3.5 < z_{\text{abs}} < 4.5$, roughly the redshift limits of this survey. More recently, Misawa et al. (2002) find 55 CIV doublets, 19 Si IV and only 3 Mg II in the spectra of 18 quasars. The CIV samples of each of these surveys are plotted in Figure 3 as a function of the CIV λ 1548 rest frame equivalent widths, W_{rest} . The change of slope of the Misawa et al. distribution at $0.15 < W_{\text{rest}} < 0.30 \text{ \AA}$ conforms to theoretical expectations of the evolution of quasar absorbers (Churchill & Vogt 2001). On the other hand, the fact that the other samples do *not* show such strong evolution indicates that they are not complete below $W_{\text{rest}} < 0.30 \text{ \AA}$. Indeed, the study of Misawa et al. (2002) is based on higher-resolution data, and therefore their sample is more complete than the previous work of Steidel (1990) explaining while results from the two surveys differ. Since our sample suffers the same problem of incompleteness as Steidel (1990), we choose to limit our analysis to doublets with $W_{\text{rest}} > 0.30 \text{ \AA}$. For a Doppler parameter $b < 20$, this corresponds to $\log N(\text{CIV}) > 14.5$ (Steidel et al., 1990). For reference, Table 2 summarises the number of absorbers in various sub-samples. Interestingly, we find proportionally more

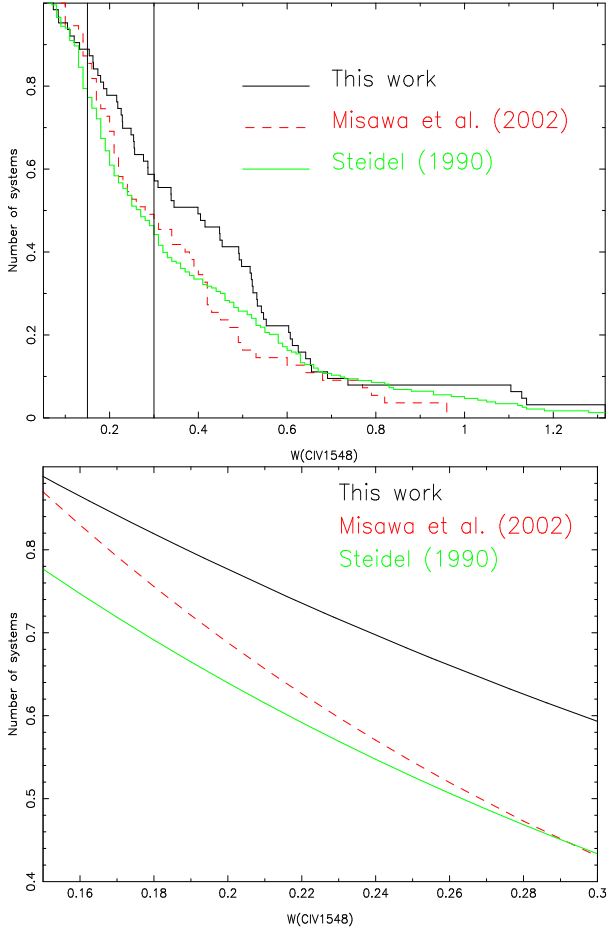


Figure 3. Top panel: Normalised cumulative distributions of CIV doublets as a function of their equivalent widths at rest, W_{rest} . The black line is for this work, the dashed light-coloured line for the Misawa et al. (2002) sample and the solid light-coloured line for Steidel (1990). The change of slope of the Misawa et al. distribution at $0.15 < W_{\text{rest}} < 0.30$ with respect to the two other samples, show that the latter are not complete at this equivalent width cut-off. Indeed, the study of Misawa et al. (2002) is based on higher-resolution data, and therefore their sample is more complete than the previous work of Steidel (1990) explaining why results from the two surveys differ. **Bottom panel:** Exponential fits to the cumulative distributions in the region of interest. The steeper slope of the Misawa et al. (2002) sample is clearly visible.

Mg II doublets than Misawa et al. (2002) but less Si IV systems, and therefore do not consider the latter absorber in our statistical analysis. We find four $W_{\text{rest}} > 1\text{Å}$ CIV absorber in our sample which demonstrates that such systems exist at $z > 3$.

5. Statistical Properties

5.1. Number Density

In order to calculate the number density, $n(z)$, of absorbers, one needs to measure the redshift path surveyed by the quasar

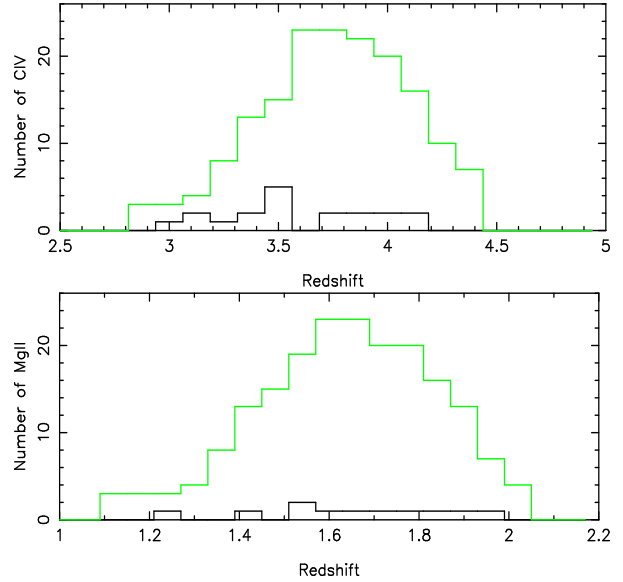


Figure 4. The light-coloured histograms represent the survey sensitivity, $g(z)$, i.e. the cumulative number of lines of sight along which a $W_{\text{rest}} > 0.30\text{Å}$ CIV (top panel) or a Mg II (bottom panel) *could* be detected at the 5σ confidence level. The black histograms are the redshift distribution of the sub-samples of $W_{\text{rest}} > 0.30\text{Å}$ CIV and Mg II, respectively.

sample. For each quasar spectrum, we compute the theoretical signal-to-noise (S/N) necessary to recover an absorber with $W_{\text{rest}} > 0.30\text{Å}$ at 5σ . After measuring the S/N in each observed spectrum, we reject 5 lines of sight: PSS J0248–1722, BR J0334–1612 and PSS J0747+4434, all observed at WHT in November 2001 when the weather conditions were extremely poor and BR J1456+2007 & PSS J1802+5616 (WHT run of June 2002). The two last columns of Table 3 give the minimum and maximum redshift for each quasar spectrum. This is illustrated by Figure 4 which shows the cumulative number of lines of sight along which a $W_{\text{rest}} > 0.30\text{Å}$ CIV (top panel) or a Mg II (bottom panel) *could* be detected at the 5σ confidence level. This is the survey sensitivity, $g(z)$, defined as follows,

$$g(z) = \sum H(z_i^{\text{max}} - z)H(z - z_i^{\text{min}}) \quad (1)$$

where H is the Heaviside step function. On the same figure the redshift distribution of the sub-samples of $W_{\text{rest}} > 0.30\text{Å}$ CIV and Mg II, respectively, are plotted.

The number density of quasar absorbers is the number of absorbers, n , per unit redshift dz , i.e., $dn/dz = n(z)$. This is a directly observable quantity, although, its interpretation is dependent on the geometry of the Universe. Indeed, the evolution of the number density of absorbers with redshift is the intrinsic evolution of the true number of absorbers combined with effects due to the expansion of the Universe. For a non-zero Λ -Universe, the expected incidence of absorbers, under the null hypothesis that there has been no evolution in number density,

Quasar	S/N	z_{\min}	z_{\max}
BR J0006–6208	20–30	3.531	4.446
BR J0030–5129	10–20	3.208	4.165
PSS J0034+1639	15–25	3.274	4.243
PSS J0133+0400	30–40	3.115	4.077
PSS J0248+1802	10–20	3.287	3.807*
BR J0311–1722	10–20	3.206	4.031
BR J0324–2918	20–30	3.621	4.471
BR J0334–1612	10–20	3.287	3.416*
		3.423	3.802*
BR J0355–3811	20–30	3.621	4.471
BR J0419–5716	10–20	3.621	4.452
BR J0426–2202	10–20	3.479	4.311
PMN J0525–3343	10–20	3.479	4.329
BR J0529–3552	20–30	3.201	4.051
BR J0714–6455	20–30	3.621	4.453
PSS J0747+4434	5–10	3.287	3.807*
PSS J1159+1337	40–50	2.788	3.889
PSS J1253–0228	15–25	2.811	3.857
PSS J1330–2522	10–20	2.807	3.887
BR J1456+2007	5–10	3.366	4.240*
BR J1618+4125	10–20	3.352	4.204
PSS J1633+1411	20–30	3.531	4.342
PSS J1646+5514	20–30	3.343	4.029
PSS J1723+2243	15–25	3.530	4.158
		4.166	4.498
PSS J1802+5616	5–15	3.351	4.149*
PSS J2154+0335	20–30	3.276	4.243
PSS J2155+1358	20–30	3.368	4.247
BR J2216–6714	20–30	3.531	4.460
PSS J2344+0342	20–30	3.209	4.174
BR J2349–3712	20–30	3.209	4.174
dz(total)			24.98
dz($W_{\text{rest}} > 0.30\text{\AA}$)			21.76

* This object was not included into the final $W_{\text{rest}} > 0.30\text{\AA}$ redshift path.

Table 3. S/N ratios and redshift path surveyed for each spectrum.

gas cross-section, kinematics or chemical content, can be described as (Tytler 1981)

$$n(z) = n_0(1+z)^2 \times (\Omega_0(1+z)^3 + \Omega_k(1+z)^2 + \Omega_\Lambda)^{-1/2} \quad (2)$$

For a flat $\Omega_\Lambda = 0.7$, $\Omega_0 = 0.3$ Universe, a non-evolving number density can be modelled with the following:

$$n(z) = n_0 \times (1+z)^2 \times (0.3 \times (1+z)^3 + 0.7)^{-1/2} \quad (3)$$

We compute the number density of $W_{\text{rest}} > 0.30\text{\AA}$ CIV (top panel of Figure 5) and compare our results with the previous determinations of Steidel (1990) and Misawa et al. (2002) at lower redshifts. It appears that in these two studies the last bin is an underestimate of $n(z)$ since no CIV doublets are detected in a range where they might be expected to be seen. Most probably these are due to the limitation of the surveys. Nevertheless, the combination of these various studies show that the number density of $W_{\text{rest}} > 0.30\text{\AA}$ CIV absorbers decreases with redshift.

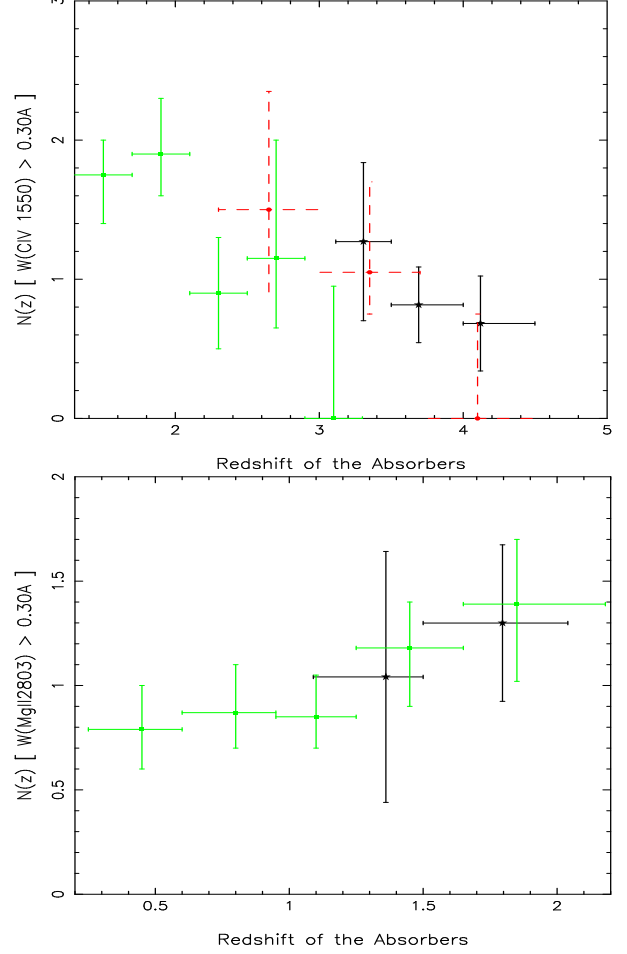


Figure 5. Number density of CIV doublets (top panel) and Mg II systems (bottom panel) at $W_{\text{rest}} > 0.30\text{\AA}$. **Top panel:** the high redshift bins are results from the present work (solid black), while Misawa et al. (2002) survey is at intermediate redshift (dashed grey) and Steidel (1990) at low redshift (solid light-coloured). **Bottom panel:** The bins covering the all redshift range (light coloured) are from Steidel & Sargent (1992) and the two bins at higher redshift are results from present work (in black).

In the bottom panel of Figure 5, we present the result of a similar computation for the $W_{\text{rest}} > 0.30\text{\AA}$ Mg II absorbers and compare it with the survey of Steidel & Sargent (1992). Both studies agree well within the error bars. In Figure 6 (top panel), we compare the number density of various classes of quasar absorbers: $W_{\text{rest}} > 0.30\text{\AA}$ CIV doublets (Steidel 1990, Misawa et al. 2002 and this work according to the redshift considered), $W_{\text{rest}} > 0.15\text{\AA}$ CIV absorbers (Misawa et al. 2002), Mg II doublets (Steidel & Sargent 1992) and LLS (Péroux et al. 2003). The first striking point from this figure is the good agreement between $W_{\text{rest}} > 0.30\text{\AA}$ Mg II absorbers and LLS number densities in the redshift range where they overlap. Indeed, both these systems are known to arise from similar regions of galaxies (Bergeron & Boissé 1991). Their number density is found to decrease with decreasing redshift. On the other hand, CIV $n(z)$ increases with time whatever the equivalent width

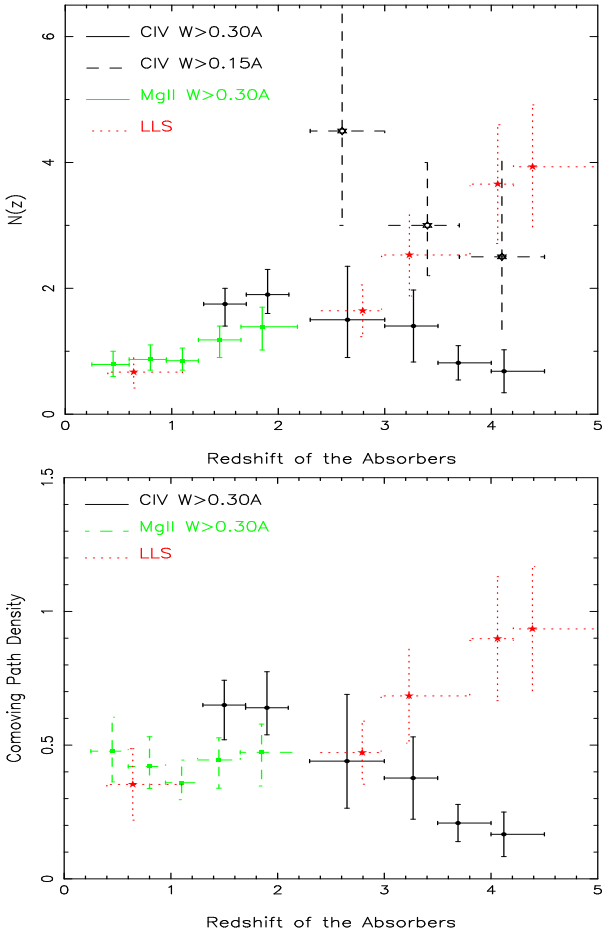


Figure 6. Top panel: number density of various class of quasar absorbers: $W_{\text{rest}} > 0.30 \text{ \AA}$ CIV doublets (Steidel 1990, Misawa et al. 2002 and this work according to the redshift considered), $W_{\text{rest}} > 0.15 \text{ \AA}$ CIV absorbers (Misawa et al. 2002), Mg II doublets (Steidel & Sargent 1992) and Lyman-limit systems (Péroux et al. 2003). **Bottom panel:** the comoving path density: this is the number of systems per comoving path length versus redshift for our assumed cosmology. A non-evolving population of absorbers should have a constant comoving path density over time.

threshold considered. Although, the number statistics are still small at $W_{\text{rest}} > 0.15 \text{ \AA}$, it is clear from Figure 6 that there are at least three times more of these systems in the Universe than $W_{\text{rest}} > 0.30 \text{ \AA}$ absorbers.

The evolution is illustrated in the bottom panel of Figure 6 where we plot the comoving path density. This is the number of systems per comoving path length versus redshift for our assumed cosmology:

$$\text{path length} = n(z) \times (0.3 \times (1+z)^3 + 0.7 \times (1+z)^2)^{1/2} \times (1+z)^{-2}$$

Therefore a non-evolving population of absorbers should have a constant comoving path density over time. We find that although this roughly holds for all absorbers at $z < 3$, above $z > 3.5$ both CIV doublets and LLS are found to depart from the horizontal line. In the region $z = 2 - 3.5$, the error bars

are still large for firm conclusions to be drawn. These results arise from both the new high redshift data now available and the use of an updated non-zero Λ -cosmology. Such an evolution is most probably the signature of the formation of halos of galaxies of size $\sim 100 h^{-1} \text{ kpc}$ from $\sim 50 h^{-1} \text{ kpc}$ systems, a process which seems to end below $z < 3$.

5.2. Metal Ratios

The CIV doublet ratio $DR = W(\text{CIV}1548)/W(\text{CIV}1550)$ probes the physical nature of the CIV absorbers. Theoretically, DR varies from 2 for the lines situated on the linear part of the curve of growth to 1 for saturated lines. Figure 7 shows the redshift evolution of DR by comparing results from Steidel (1990) at low redshift with results from our sample for CIV doublets at $z > 3.5$, both with $W_{\text{rest}}(\text{CIV}1548) > 0.30 \text{ \AA}$. In order to enable comparison with previous work, doublets which are separated by less than 1000 km s^{-1} are merged together and their equivalent width is combined. This is based on the possibility that clustered components are not physically independent and that the number of components seen is sensitive to the spectrum quality. Our resulting sample is composed of 37 CIV doublets with $W_{\text{rest}}(\text{CIV}1548) > 0.30 \text{ \AA}$ (note that this is more than in Table 2 since in that case it is $W_{\text{rest}}(\text{CIV}1550) > 0.30 \text{ \AA}$ which is used as a criterion). We note that the trend revealed by Steidel (1990) (i.e. a decrease of DR with decreasing redshift) already started at earlier times ($z \sim 4$). Assuming that DR and W are uncorrelated, this could be due to either a decrease in the mean Doppler parameter, b or to an increase in the mean column density, $N(\text{CIV})$, as time goes on. As pointed out for previous samples (Steidel 1990), we find that DR in our survey is not correlated with $W_{\text{rest}}(\text{CIV}1548)$, and therefore is not expected to be correlated with the line kinematics, parameterised by b in the range of column densities studied here. This means that the evolution we probe in Figure 7 is probably not due to a change in b , but rather to a systematic increase in the mean column density with time.

The evolution in the mean column density of CIV absorbers could be interpreted as due to a change in the chemical abundance of carbon (Songaila 2001 and Pettini et al. 2003). Another viable explanation for the observed DR evolution is a possible change in ionization state of the carbon absorbers over time, possibly due to the evolution in the ionization continuum.

In Figure 8 we plot the ratio $W(\text{Si IV}1393)/W(\text{CIV}1548)$ for the few systems in our sample which contain both these doublets. This result is shown together with the same measurement undertaken at lower redshift by Bergeron & Ikeuchi (1990). To facilitate comparison, we limit our sample to pairs with $W_{\text{rest}}(\text{CIV}1548) \geq 0.50 \text{ \AA}$ which corresponds to only 9 systems. We find that the ratio $W(\text{Si IV}1393)/W(\text{CIV}1548)$ is approximately constant from $z = 3.5$ to $z = 2.5$. At $z < 3.5$, the trend might be interpreted as evidence for a systematic increase in the ionization state of the gas. In other words, this is the opposite trend to what one would expect given the observed evolution of the CIV mean column density. Nevertheless, it should be emphasized that in order to compare with previous work from Bergeron & Ikeuchi (1990), we had to limit the

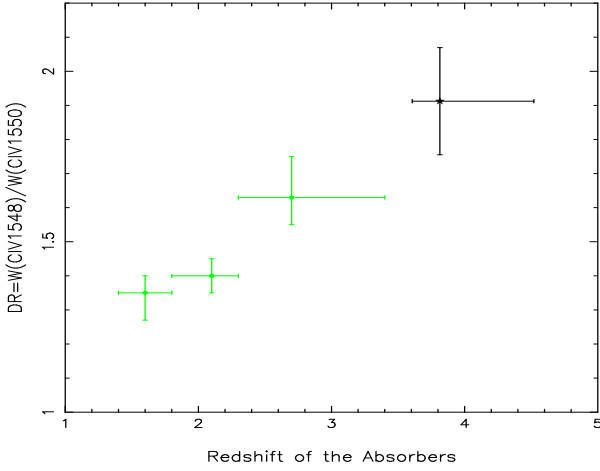


Figure 7. Redshift evolution of the doublet ratio $DR = W(\text{CIV}1548)/W(\text{CIV}1550)$ at $W_{\text{rest}}(\text{CIV}1548) > 0.30 \text{ \AA}$. The high-redshift bin is the result from the present work (in black). The three low redshift data points (light-coloured) are from Steidel (1990).

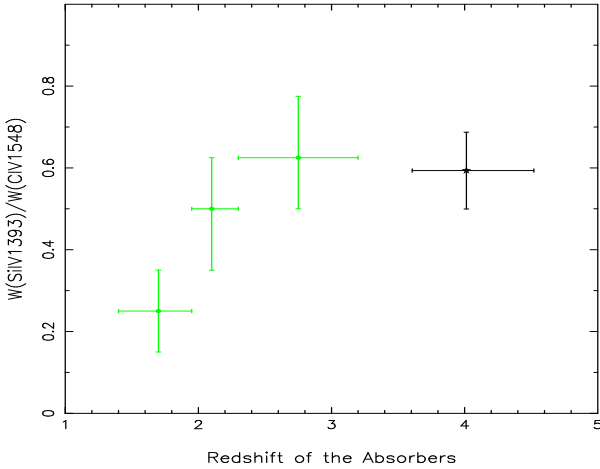


Figure 8. Redshift evolution of the ratio $W(\text{SiIV}1393)/W(\text{CIV}1548)$ at $W_{\text{rest}}(\text{CIV}1548) \geq 0.50 \text{ \AA}$. The high-redshift bin is the result from the present work (in black). The three low redshift data points (light-coloured) are from Bergeron & Ikeuchi (1990).

sample studied to $W_{\text{rest}}(\text{CIV}1548) \geq 0.50 \text{ \AA}$. These systems might not be affected by the ionization continuum in the same way as $W_{\text{rest}}(\text{CIV}1548) \geq 0.30 \text{ \AA}$ lines. Indeed, other independent lines of evidence based on: absorption temperature (Schaye et al. 2000); mean continuum depression in quasars (Bernardi et al. 2003, Theuns et al. 2002); and ionization level of sensitive elements in quasar absorbers (Vladilo et al. 2003), seem to favour the scenario where the He II reionization takes place around $z \sim 3.2$. Therefore, a change of $W(\text{SiIV}1393)/W(\text{CIV}1548)$ ratio is expected around this redshift, either side of which, the ratio should remain fairly flat, not what we observe in Figure 8. Songaila (1998) found such trends in high-resolution quasar spectra, but her results were not con-

firmed by Kim, Cristiani & D’Odorico (2002) from comparably high quality data.

To summarise, we observe a decrease of C IV doublet DR as time goes on. This evolution is interpreted as the signature of an increase in the mean C IV column density possibly linked with chemical evolution or/and with changes in the ionization state of the absorbers.

6. Conclusion

We have presented a new sample of high-redshift quasar absorbers gathered from observations undertaken at the WHT for the northern objects and at ESO/NTT for the southern ones. These data are analysed in conjunction with previous studies in order to clarify the statistical properties of a number of metal lines and link these with the evolution of galactic structures. Our main findings can be summarised as follow:

- The apparent disagreement between the $n(z)$ redshift evolution of C IV at $W_{\text{rest}}(\text{CIV}) > 0.15 \text{ \AA}$ reported by Misawa et al. (2002) from a comparison with Steidel (1990), is the result of different completeness levels in the absorber samples.
- The number density of $W_{\text{rest}}(\text{CIV}) > 0.30 \text{ \AA}$ C IV doublets increases with decreasing redshift from $z \sim 4.5$. $W_{\text{rest}}(\text{CIV}) > 0.15 \text{ \AA}$ C IV systems are more numerous than the former at all redshifts. On the other hand, $n(z)$ of $W_{\text{rest}}(\text{Mg II}) > 0.30 \text{ \AA}$ Mg II doublets and LLS follow each other and decreases as time goes on.
- At $z > 3$, the LLS population is predominant while the number of $W_{\text{rest}}(\text{CIV}) > 0.30 \text{ \AA}$ C IV is increasing with time. Below $z < 3$, none of all the classes of absorbers show signs of evolution. We interpret this as the formation of galactic envelopes from smaller halos.
- The doublet ratio $DR = W(\text{CIV}1548)/W(\text{CIV}1550)$ is found to decrease with decreasing redshift, a signature of the increase of the mean C IV column density.
- A study of the $W(\text{SiIV}1393)/W(\text{CIV}1548)$ ratio for strong absorbers ($W_{\text{rest}}(\text{CIV}1548) \geq 0.50 \text{ \AA}$) shows a flattening at $z > 3.5$, followed by a decrease, counter to the scenario in which the DR trend can be explained by a change in ionization continuum.

Acknowledgments

We would like to thank Jacqueline Bergeron for comments on an earlier version of the manuscript. CP is supported by a Marie Curie fellowship. This work was supported in part by the European Communities RTN network “The Physics of the Intergalactic Medium”. This paper is based on observations obtained at the William Herschel Telescope which is operated on the island of La Palma by the Isaac Newton Group in the Spanish Observatorio del Roque de los Muchachos of the Instituto de Astrofísica de Canarias, and on observations collected during programme ESO 68.A-0279 and ESO 69.A-0541 at the European Southern Observatory with EMMI on NTT operated at La Silla Observatory, Chile.

References

- Adelberger, K.L., Steidel, C.C., Shapley, A.E. & Pettini, M., 2003, *ApJ*, 584, 45.
- Bergeron, J. & Ikeuchi, S., 1990, *A&A*, 235, 8.
- Bergeron, J. & Boissé, P., 1991, *A&A*, 243, 344.
- Bernardi, M. & the SDSS collaboration, 2003, *AJ*, 125, 32.
- Boksenberg, A., Sargent, W.L.W. & Rauch, M., 2003, *ApJS*, *submitted (astro-ph/0308557)*.
- Chen, H-W, Lanzetta, K. & Webb, J., 2001, *ApJ*, 556, 158.
- Churchill, C.W., Rigby, J.R., Charlton, J.C., Vogt, S.S., 1999, *ApJS*, 120, 51.
- Churchill, C.W. & Vogt, S.S., 2001, *AJ*, 122, 679.
- Crotts, A., Burles, S. & Tytler, D., 1997, *ApJ*, 489, 7.
- Ellison, S., Songaila, A., Schaye, J. & Pettini, M., 2000, *AJ*, 120, 1175.
- Haehnelt, M., Steinmetz, M. & Rauch, M., 1996, *ApJL*, 465, 95.
- Kim, T.S., Cristiani, S. & D'Odorico, S., 2002, *A&A*, 383, 747.
- Quashnock, J., Vanden Berk, D. & York, D., 1996, *ApJ*, 472, 69.
- Misawa, T., Tytler, D., Iye, M., Storrie-Lombardi, L., Suzuki, N. & Wolfe, A.M., 2002, *AJ*, 123, 1847.
- Péroux, C., Storrie-Lombardi, L.J., McMahon, R.G., Irwin, M., & Hook, I.M., 2001, *AJ*, 121, 1799.
- Péroux, C., McMahon, R.G., Storrie-Lombardi, & L.J., Irwin, 2003, *MNRAS*, 346, 1103.
- Petitjean, P. & Bergeron, J. 1994, *A&A*, 283, 759.
- Pettini, M., Madau, P., Bolte, M., Prochaska, J., Ellison, S. & Fan, X., 2003, *AJ*, 594, 695.
- Rauch, M., Sargent, W., Womble, D. & Barlow, T., 1996, *ApJ*, 467, L5.
- Sargent, W., Boksenberg, A. & Steidel, C., 1988, *ApJS*, 68, 539.
- Schaye, J., Theuns, T., Rauch, M., Efstathiou, G., & Sargent, W.L.W., 2000, *MNRAS*, 318, 817.
- Songaila, A., 1998, *AJ*, 115, 218.
- Songaila, A., 2001, *ApJ*, 561, L153.
- Steidel, C., 1990, *ApJS*, 71, 1.
- Steidel, C. & Sargent, W., 1992, *ApJSS*, 80, 1.
- Theuns, T., Schaye, J., Zaroubi, S., Kim, T.S., Tzanavaris, P. & Carswell, R., 2002, *ApJ*, 567, L103.
- Tytler, D., 1981, *Nature*, 291, 289.
- Vladilo, G., Centurión, M., D'Odorico, V. & Péroux, C., 2003, *A&A*, 402, 487.

Appendix A: Metal Line Identification

All detected absorptions with confirmed identifications are listed in Table A.1 below for each quasar spectrum.

Quasars	z_{em}	λ_{obs}	z_{abs}	W_{obs}	W_{rest}	Identification
BR J0006-6208	4.455	7021.28	1.956	2.08	0.70	FeII 2374
		7046.45	1.956	3.55	1.20	FeII 2382
		7103.95	3.588	2.44	0.53	CIV 1548
		7120.51	3.588	1.20	0.26	CIV 1550
		7158.94	3.588	1.07	0.23	CI 1560
		7438.79	1.956	0.67	0.23	SiII 2515
		7513.67	1.687	0.67	0.25	MgII 2796
		7533.75	1.687	0.16	0.06	MgII 2803
		7648.54	1.956	3.05	1.03	FeII 2586
		7686.24	1.956	3.96	1.34	FeII 2600
		8040.22	1.956	4.19	1.42	if real FeI 2719
		8268.55	1.956	5.79	1.96	MgII 2796 sat
		8289.04	1.956	5.12	1.73	MgII 2803 sat
		8435.04	1.956	1.22	0.41	MgI 2852
BR J0030-5129	4.174	6913.48	3.465	1.38	0.31	CIV 1548
		6925.59	3.465	0.96	0.22	CIV 1550
PSS J0034+1639	4.293	6663.26	1.798	4.71	1.68	FeII 2382
		6816.75	4.225	0.88	0.17	SiII 1304
		6836.35	3.478	0.99	0.22	SiII 1526
		6877.33	3.442	3.07	0.69	CIV 1548
		6888.96	3.442	2.82	0.63	CIV 1550
		6935.49	3.478	2.74	0.61	CIV 1548 (3.442 CI 1560)
		6944.17	3.478	1.61	0.36	CIV 1550 (4.225 CI 1328)
		7237.51	1.588	2.17	0.84	MgII 2796 (1.798 FeII 2586)
		7254.15	1.588	0.93	0.36	MgII 2803
		7279.15	1.798	4.61	1.65	FeII 2600
		7824.35	1.798	4.69	1.68	MgII 2796 sat
		7844.70	1.798	3.94	1.41	MgII 2803
		8062.75	1.883	2.57	0.89	MgII 2796
		8082.71	1.883	1.04	0.36	MgII 2803
8087.25	4.225	2.37	0.45	CIV 1548		
8103.07	4.225	1.30	0.25	CIV 1550		
PSS J0133+0400	4.154	6372.36	3.771	5.23	1.10	CII 1334
		6406.40	3.138	4.57	1.10	CIV 1548
		6416.68	3.138	2.79	0.67	CIV 1550
		6438.17	3.620	1.13	0.24	SiIV 1393
		6479.49	3.620	1.11	0.24	SiIV 1402
		6507.30	3.996	1.63	0.33	OI 1302
		6514.00	3.996	0.53	0.11	SiII 1304
		6545.49	3.229	0.76	0.18	CIV 1548 (4.110 CI 1280)
		6555.91	3.229	0.44	0.10	CIV 1550
		6648.55	3.771	2.11	0.44	SiIV 1393
		6663.09	4.110	1.69	0.33	SiII 1304
		6691.32	3.771	1.11	0.23	SiIV 1402
		6894.13	1.664	2.36	0.89	FeII 2586
		6929.30	1.664	3.26	1.22	FeII 2600
		6962.01	3.992	2.88	0.58	SiIV 1393
		7005.36	3.992	1.19	0.24	SiIV 1402
		7121.44	4.110	0.61	0.12	SiIV 1393
		7128.77	4.115	1.94	0.38	SiIV 1393
		7167.68	4.110	0.62	0.12	SiIV 1402
		7174.99	4.115	1.24	0.24	SiIV 1402
7281.79	3.771	4.46	0.93	SiII 1526		
7385.12	3.771	2.88	0.60	CIV 1548		
7397.15	3.771	1.58	0.33	CIV 1550		

Quasars	z_{em}	λ_{obs}	z_{abs}	W_{obs}	W_{rest}	Identification
		7449.89	1.664	4.32	1.62	MgII 2796 sat
		7469.08	1.664	4.11	1.54	MgII 2803 sat
		7604.01	1.664	2.05	0.77	MgI 2852
		7671.08	3.771	3.10	0.65	FeII 1608
		7728.49	3.992	1.69	0.34	CIV 1548
		7735.34	3.996	1.43	0.29	CIV 1548
		7742.27	3.992	0.89	0.18	CIV 1550
		7747.94	3.996	0.65	0.13	CIV 1550
		7810.29	4.115	0.43	0.08	SiII 1526
PSS J0248+1802	4.422	6909.82	1.470	3.46	1.40	MgII 2796
		6926.86	3.969	0.95	0.19	SiIV 1393 (1.470 MgII 2803)
		6970.76	3.969	0.30	0.06	SiIV 1402
		7227.49	4.185	1.29	0.25	SiIV 1393
		7275.61	4.185	0.86	0.17	SiIV 1402
BR J0311-1722	4.039	6553.53	4.034	0.46	0.09	OI 1302
		7794.11	4.034	6.63	1.32	CIV 1548 assym profiles
		7808.10	4.034	2.37	0.47	CIV 1550
BR J0324-2918	4.622	7347.10	3.746	0.57	0.12	CIV 1548
		7359.84	3.746	0.72	0.15	CIV 1550
		7564.20	2.227	0.91	0.28	FeII 2344
		7691.00	2.227	1.42	0.44	FeII 2382
		8176.73	1.923	1.33	0.46	MgII 2796
		8196.15	1.923	0.64	0.22	MgII 2803
		8345.80	2.227	0.77	0.24	FeII 2586
		8392.62	2.227	1.36	0.42	FeII 2600
BR J0334-1612	4.363	6673.26	3.788	1.05	0.22	SiIV 1393
		6713.80	3.788	0.57	0.12	SiIV 1402
		7228.38	3.668	1.07	0.23	CIV 1548 (4.186 SiIV 1393)
		7239.12	3.668	0.37	0.08	CIV 1550
		7275.85	4.186	1.93	0.37	SiIV 1402
		7368.97	3.759	1.61	0.34	CIV 1548
		7381.79	3.759	0.81	0.17	CIV 1550
BR J0355-3811	4.545	7516.08	3.855	0.51	0.11	CIV 1548
		7528.44	3.855	0.59	0.12	CIV 1550
		7723.51	1.986	2.09	0.70	FeII 2586
		7764.48	1.986	3.49	1.17	FeII 2600
		8226.45	4.313	2.88	0.54	CIV 1548
		8233.01	4.318	3.92	0.74	CIV 1548
		8239.86	4.313	1.02	0.19	CIV 1550
		8248.49	4.318	1.06	0.20	CIV 1550
		8349.70	1.986	10.28	3.42	MgII 2796
		8371.16	1.986	9.38	3.14	MgII 2803
BR J0419-5716	4.461	7217.62	2.028	2.45	0.81	FeII 2382
		7834.70	2.028	1.51	0.50	FeII 2586
		7875.67	2.028	2.30	0.76	FeII 2600
		8080.50	4.218	2.73	0.52	CIV 1548
		8095.89	4.218	1.49	0.29	CIV 1550
		8225.50	4.311	3.32	0.63	CIV 1548
		8239.86	4.311	0.97	0.18	CIV 1550
		8411.29	4.434	0.60	0.11	CIV 1548
		8426.32	4.434	0.44	0.08	CIV 1550
		7132.42	3.606	5.20	1.13	CIV 1548
		7143.72	3.606	3.25	0.71	CIV 1550
		7209.92	4.172	2.08	0.40	SiIV 1393
		7249.67	3.682	1.07	0.23	CIV 1548
		7255.61	4.172	2.10	0.41	SiIV 1402
		7261.58	3.682	0.82	0.18	CIV 1550
		8007.87	4.172	3.14	0.61	CIV 1548
		8020.81	4.172	1.88	0.36	CIV 1550
BR J0426-2202	4.320	7132.42	3.606	5.20	1.13	CIV 1548
		7143.72	3.606	3.25	0.71	CIV 1550

Quasars	z_{em}	λ_{obs}	z_{abs}	W_{obs}	W_{rest}	Identification
		7209.92	4.172	2.08	0.40	SiIV 1393
		7249.67	3.682	1.07	0.23	CIV 1548
		7255.61	4.172	2.10	0.41	SiIV 1402
		7249.67	3.682	1.07	0.17	CIV 1548
		8007.87	4.172	3.14	0.61	CIV 1548
		8020.81	4.172	1.88	0.36	CIV 1550
PMN J0525–3343	4.383	7057.43	4.063	0.65	0.13	SiIV 1393
		7093.42	3.581	1.00	0.22	CIV 1548 (4.063 SiIV 1402)
		7104.99	3.581	0.78	0.17	CIV 1550
		7182.54	1.568	3.05	1.19	MgII 2796
		7201.04	1.568	3.19	1.24	MgII 2803
		7367.39	3.581	0.92	0.20	FeII 1608
		7569.07	4.430	3.40	0.63	SiIV 1393
		7618.63	4.430	4.57	0.84	SiIV 1402
		7729.29	4.063	1.36	0.27	SiII 1526
		7841.89	4.063	1.45	0.29	CIV 1548
		7854.16	4.063	0.68	0.13	CIV 1550
		8145.68	4.063	0.80	0.16	FeII 1608
		225.917	4.313	3.48	0.65	CIV 1548
		8239.63	4.313	0.46	0.09	CIV 1550
BR J0529–3552	4.172	6605.73	4.062	1.42	0.28	SiII 1304
		6708.94	1.398	1.20	0.50	MgII 2796
		6726.52	1.398	0.57	0.24	MgII 2803
		6759.82	4.062	0.49	0.10	CII 1334
		6779.25	1.423	0.87	0.36	MgII 2796
		6795.07	1.423	0.77	0.32	MgII 2803
		6973.94	3.503	2.40	0.53	CIV 1548
		6985.50	3.503	1.39	0.31	CIV 1550
		7058.81	4.062	1.84	0.36	SiIV 1393
		7103.20	4.062	1.45	0.29	SiIV 1402
		7244.21	3.503	1.48	0.33	FeII 1608
		7427.65	1.656	0.91	0.34	MgII 2796
		7449.85	1.656	1.20	0.45	MgII 2803
		7528.19	3.503	1.00	0.22	AlII 1670
		7729.91	4.062	0.94	0.19	SiII 1526
BR J0714–6455	4.462	7238.83	4.193	0.85	0.16	SiIV 1393
		7248.78	3.747	1.03	0.22	SiII 1526 (4.193 SiIV 1402)
		7350.31	3.747	1.97	0.41	CIV 1548
		7362.34	3.747	0.74	0.16	CIV 1550
		7689.35	3.966	2.58	0.52	CIV 1548
		7701.69	3.966	2.04	0.41	CIV 1550
		8040.53	4.193	2.55	0.49	CIV 1548
		8053.67	4.193	1.17	0.23	CIV 1550
PSS J0747+4434	4.430
PSS J1159+1337	4.073	6418.61	1.739	1.09	0.40	FeII 2344
		6502.11	1.739	0.43	0.16	FeII 2374
		6522.56	1.739	1.83	0.67	FeII 2382
		6582.48	3.724	1.24	0.26	SiIV 1393
		6625.76	3.756	1.11	0.23	SiIV 1393 (3.724 SiIV 1402)
		6670.04	3.756	0.34	0.07	SiIV 1402
		7081.73	1.739	0.75	0.27	FeII 2586
		7119.62	1.739	1.64	0.60	FeII 2600
		7311.64	3.724	1.02	0.22	CIV 1548
		7323.59	3.724	0.42	0.09	CIV 1550
PSS J1253+0228	4.007	6142.86	3.606	1.23	0.27	CII 1334
		6320.60	1.261	2.22	0.98	MgII 2796
		6335.10	1.261	0.89	0.39	MgII 2803
		6415.92	3.606	4.98	1.08	SiIV 1393
		6458.09	3.606	3.89	0.84	SiIV 1402
		7127.23	3.606	5.25	1.14	CIV 1548
		7139.24	3.606	4.16	0.90	CIV 1550

Quasars	z_{em}	λ_{obs}	z_{abs}	W_{obs}	W_{rest}	Identification
BR J1330–2522	3.949	6319.29	3.084	2.01	0.49	CIV 1548
		6329.36	3.084	1.51	0.37	CIV 1550
		6645.79	3.772	0.78	0.16	SiIV 1393
		6689.87	3.772	0.32	0.07	SiIV 1402
		6794.58	3.390	0.85	0.19	CIV 1548
		6805.62	3.390	0.81	0.18	CIV 1550
		6819.10	3.084	1.38	0.34	AlII 1670
		6874.38	3.440	1.55	0.35	triplet
		7383.72	3.769	1.93	0.40	CIV 1548
		7395.73	3.769	1.64	0.34	CIV 1550
PSS 1456+2007	4.249	7720.09	1.761	0.95	0.34	MgII 2796
		7740.89	1.761	0.70	0.25	MgII 2803
		7796.79	4.036	1.25	0.25	CIV 1548
		7807.97	4.036	0.58	0.12	CIV 1550
0.11 PSS J1618+4125	4.213	7276.55	4.223	0.60		SiIV 1393
		7382.46	4.223	0.57	0.11	SiIV 1402
0.16 PSS J1633+1411	4.351	7091.98	3.580	0.75		CIV 1548
		7104.05	3.580	0.40	0.09	CIV 1550
		7179.44	4.150	0.96	0.19	SiIV 1393
		7225.18	4.150	0.70	0.14	SiIV 1402
		8177.34	4.282	2.37	0.45	CIV 1548
		8192.78	4.282	1.573	0.30	CIV 1550
PSS J1646+5514	4.037	6988.64	3.516	0.23	0.05	CIV 1548
		7000.70	3.516	0.33	0.07	CIV 1550 (3.521 CIV 1548)
		7010.49	4.030	0.89	0.18	SiIV 1393 (3.521 CIV 1550)
		7033.53	3.544	2.26	0.50	CIV 1548
		7045.50	3.544	1.40	0.31	CIV 1550
		7055.81	4.030	0.48	0.10	SiIV 1402
		7357.65	3.754	1.43	0.30	CIV 1548
		7366.80	3.759	0.40	0.08	CIV 1548
		7369.19	3.754	1.11	0.23	CIV 1550
		7378.21	3.759	0.14	0.03	CIV 1550
		7678.92	4.030	0.65	0.13	SiII 1526
		7786.91	4.030	1.39	0.28	CIV 1548
		7797.52	4.037	1.28	0.25	CIV 1548
		7798.54	4.030	2.38	0.47	CIV 1550
		7809.73	4.037	0.44	0.09	CIV 1550
		7994.39	1.859	0.92	0.32	MgII 2796
8015.44	1.859	0.51	0.18	MgII 2803		
8089.58	4.030	0.14	0.03	FeII 1608		
PSS J1723+2243	4.520	7065.98	3.696	0.69	0.15	SiII 1526 (dbl cpt)
		7283.89	3.704	3.02	0.64	CIV 1548
		7296.29	3.704	1.29	0.27	CIV 1550
		7311.00	4.244	1.20	0.23	SiIV 1393
		7355.29	4.244	0.49	0.09	SiIV 1402
		7550.54	3.696	1.51	0.32	FeII 1608 (dbl cpt)
		7843.36	3.696	2.67	0.57	AlII 1670 (dbl cpt)
		8004.04	4.244	0.83	0.16	SiII 1526
		8104.95	4.234	0.85	0.16	CIV 1548
		8117.52	4.244	1.81	0.35	CIV 1548
		8120.59	4.234	1.52	0.29	CIV 1550
		8137.92	4.244	0.77	0.15	CIV 1550
PSS J1802+5616	2.891	7035.30	4.048	0.69	0.14	SiIV 1393
		7080.97	4.048	0.50	0.10	SiIV 1402 (3.651 SiII 1526)
		8035.92	4.190	1.33	0.26	CIV 1548
		8047.76	4.190	0.44	0.08	CIV 1550

Quasars	z_{em}	λ_{obs}	z_{abs}	W_{obs}	W_{rest}	Identification
PSS J2154+0335	4.363	6912.21	3.961	1.07	0.22	SiIV 1393
		6958.06	3.961	0.79	0.16	SiIV 1402
		7127.54	1.756	1.72	0.62	FeII 2586
		7168.48	1.756	3.33	1.21	FeII 2600
		7531.09	3.776	0.89	0.19	CIV 1548
		7545.17	3.776	1.00	0.21	CIV 1550 cont
		7681.74	3.961	1.98	0.40	CIV 1548
		7694.48	3.961	1.47	0.30	CIV 1550
		7706.41	1.756	4.68	1.70	MgII 2796 sat
		7727.70	1.756	4.49	1.63	MgII 2803 sat
		7865.25	1.756	1.07	0.39	MgI 2852
PSS J2155+1358	4.256	6943.22	1.914	2.23	0.77	FeII 2382
		7067.67	3.567	2.98	0.65	CIV 1548
		7079.20	3.567	2.02	0.44	CIV 1550
		7308.18	4.244	2.15	0.41	SiIV 1393
		7354.97	4.244	2.28	0.43	SiIV 1402
		7538.26	1.914	0.42	0.14	FeII 2586
		7579.07	1.914	1.33	0.46	FeII 2600
		8117.54	4.244	2.90	0.55	CIV 1548 sat
		8131.14	4.244	2.22	0.42	CIV 1550 sat
		8148.42	1.914	5.16	1.77	MgII 2796 sat
		8170.12	1.914	5.08	1.74	MgII 2803 sat
BR J2216-6714	4.469	7173.70	2.060	3.29	1.08	FeII 2344
		7268.79	2.060	2.43	0.79	FeII 2374
		7295.82	2.060	3.61	1.18	FeII 2382
		7320.39	3.728	0.82	0.17	CIV 1548
		7333.77	3.728	0.70	0.15	CIV 1550
		7367.07	4.285	0.84	0.16	SiIV 1393
		7413.73	4.285	0.68	0.13	SiIV 1402
		7491.72	3.837	0.64	0.13	CIV 1548
		7503.76	3.837	0.47	0.10	CIV 1550
		7607.87	3.728	0.40	0.08	FeII 1608
		7889.88	4.095	1.30	0.26	CIV 1548
		7902.97	4.095	0.33	0.06	CIV 1550
		7914.40	2.060	3.09	1.01	FeII 2586
		7956.90	2.060	4.44	1.45	FeII 2600
PSS J2344+0342	4.239	6531.04	3.219	2.20	0.52	CIV 1548
		6542.17	3.219	2.04	0.48	CIV 1550
		6589.50	4.053	0.88	0.17	SiII 1304
		6789.50	3.219	1.81	0.43	FeII 1608
		6805.74	3.882	1.52	0.31	SiIV 1393
		6849.34	3.882	1.31	0.27	SiIV 1402
		7050.98	3.219	2.93	0.69	AlII 1670
		7453.44	3.882	0.75	0.15	SiII 1526
		7559.01	3.882	2.67	0.55	CIV 1548
		7571.64	3.882	1.56	0.32	CIV 1550
		7714.09	4.053	0.54	0.11	SiII 1526
		7824.45	4.053	0.43	0.09	CIV 1548
				7836.06	4.053	0.22
BR J2349-3712	4.208	6538.49	3.690	1.23	0.26	SiIV 1393 (3.284 SiII 1526)
		6581.17	3.690	0.93	0.20	SiIV 1402
		6592.52	3.258	2.20	0.52	CIV 1548
		6603.81	3.258	1.34	0.31	CIV 1550
		6632.13	3.284	0.66	0.15	CIV 1548
		6643.93	3.284	0.54	0.13	CIV 1550
		6891.96	3.284	0.99	0.23	FeII 1608
				7161.63	3.284	0.77

Quasars	z_{em}	λ_{obs}	z_{abs}	W_{obs}	W_{rest}	Identification
		7267.37	3.690	1.06	0.23	CIV 1548
		7274.45	3.690	0.78	0.17	CIV 1550
		7364.09	3.757	2.13	0.45	CIV 1548
		7377.16	3.757	1.60	0.34	CIV 1550
		7679.67	3.960	1.54	0.31	CIV 1548
		7694.11	3.960	0.61	0.12	CIV 1550
		7714.71	1.758	1.01	0.37	MgII 2796
		7734.25	1.758	0.35	0.13	MgII 2803
		7832.95	3.690	1.30	0.28	AlIII 1670

*Object possibly affected by BAL features.

Table A.1. List of detected absorption lines which are successfully identified with observed wavelength, equivalent width, and corresponding absorption redshift.